ELSEVIER

Earth and Planetary Science Letters 210 (2003) 527–543

EPSL

www.elsevier.com/locate/epsl

Joint bulk-sound and shear tomography for Western Pacific subduction zones

A. Gorbatov *, B.L.N. Kennett

Research School of Earth Sciences, The Australian National University, Canberra, ACT 0200, Australia

Received 30 September 2002; received in revised form 4 March 2003; accepted 14 March 2003

Abstract

Detailed regional body wave tomographic inversion of the Western Pacific region has been performed using P and S travel times from common sources and receivers, with a joint inversion in terms of bulk-sound and shear wave-speed variations in the mantle. This technique allows the separation of the influence of bulk and shear moduli, and hence a more direct comparison with mineral physics information. The study region is parameterized with cells of side 0.5° to 2° and 19 layers to a depth of 1500 km, while the rest of the mantle was parameterized with $5\times5°$ cells with 16 layers between the surface and the core–mantle boundary. A simultaneous inversion is made for regional and global structures to minimize the influence of surrounding structures on the regional image. A nested iterative inversion scheme is employed with local linearization and three-dimensional ray tracing through the successive model updates. The results of the regional tomographic inversion reveal the penetration of a subducted slab below the 660 km discontinuity at the Kurile–Kamchatka trench, while flattening of slabs above this depth is observed in the Japan and Izu–Bonin subduction zones on both the bulk-sound and shear wave-speed images. The penetration of a subducted slab down to a depth of at least 1200 km is seen below the southern part of the Bonin trench, Mariana, Philippine, and Java subduction zones. Fast shear wave-speed perturbations associated with the subducted slabs, down to the 410 km transition zone, are larger than the comparable bulk-sound perturbations for all these subduction zones except the Philippines. The bulk-sound signature for the subducted slab is more pronounced than for shear in the Philippines, Talaud, New Guinea, Solomon, and Tonga subduction zones, where penetration of the slab into the middle mantle is observed. Variation in the amplitude ratio between bulk-sound and shear wave-speed anomalies correlates well with the subduction parameters of the descending slab. Slabs younger than 90 Ma at the trench show bulk-sound dominance in the upper mantle, while older slabs have a stronger shear wave-speed signature. Spreading of the fast shear wave-speed zone between 800 and 1000 km is observed in the areas of deep subducted slab penetration, but has no comparable expression in the bulk-sound images. This high-velocity feature may reflect physical or chemical disequilibria introduced to the lower mantle by subducted slabs.

Keywords: seismic tomography; subduction zone; P waves; S waves

1. Introduction

Tomographic techniques for Earth probing have proved to be one of the most powerful tools

* Corresponding author. Present address: IFREE, JAMSTEC, 2-15 Natsushima-cho, Yokosuka 237-0061, Japan.
E-mail address: alexei@jamstec.go.jp (A. Gorbatov).

0012-821X/03/$ – see front matter
doi:10.1016/S0012-821X(03)00165-1

of modern geophysical research. Starting from small-scale studies [1] the technique has developed to recent high-resolution global studies [2–4] in which researchers try to infer the inner structure of the Earth through estimation of the three-dimensional distribution of seismic wave-velocity anomalies. The aim of much tomographic inversion has been to reconstruct the tectonic history of the Earth or the peculiarities of modern tectonic processes (e.g. [2,5–9]). Only recently the analysis of tomographic models has focused on the estimation of the physical properties of the Earth's mantle (e.g. [10–13]). A significant advance in these studies has come from the comparison of bulk-sound speed and shear wave-speed anomalies obtained from a joint P and S data inversion [10] and attempts to compare P and S wave-speed tomograms (e.g. [13–15]).

When attention is confined to P and S wave data which have equivalent path coverage, it is possible to use the relative size of the bulk-sound speed and shear wave-speed anomalies to reveal the nature of seismic heterogeneity. This is particularly valuable for investigation of the physical properties in subduction processes, because the sources in the slab itself improve the sampling of the region. Widiyantoro et al. [13] suggest the dominance of shear wave-speed anomalies in the rigid subducted slabs penetrating into the lower mantle, whereas dominance of bulk-sound anomalies is an indicator of low flexural rigidity in bent or stagnant slabs lying above the 660 km discontinuity. This observation, based mostly on the analysis of the Izu–Bonin and Tonga subduction zones, provides new possibilities for the understanding of the physical properties in the Earth. However, it is possible that these striking results could be a feature of the geometry and tectonic environment of the regions studied, rather than a characteristic of the subduction process.

We therefore undertake a comprehensive analysis of the Western Pacific region, which contains much of the world's subduction zones, using high-resolution joint inversion of P and S arrival-time data to generate tomographic images of bulk-sound speed and shear wave-speed variation. We focus attention on the relative amplitudes of the bulk-sound and shear wave-speed anomalies and their relation to the nature of the descending subducted plates in a region with a wide range of different slab environments.

2. Data and method

We use the global catalog of event locations and phase arrival times of Engdahl et al. [16], incorporating subsequent updates. This catalog is derived from bulletin data with iterative reprocessing and relocation of events using the ak135 model [17] and subsequent re-association of phase identifications. The incorporation of depth-phase information helps to improve the accuracy of the hypocentral information.

Only P and S arrival times with source and receiver in common were selected to ensure as close a match as possible between the ray paths traversed by the P and S waves. Within the Western Pacific region we have included all available pairs of P and S times. The regional structure is represented with 19 layers in depth, with cells of size $0.5\times0.5°$ in the uppermost mantle, $1\times1°$ in the transition zone and lower mantle, and $2\times2°$ below continents down to a depth of 1500 km. In order to reduce the size of the system of equations that needs to be solved, we have used a coarser parametrization for the rest of the mantle. In the mantle surrounding the Western Pacific region we used 16 layers of $5\times5°$ cells, and cumulated P and S path information into station–event clusters with a size of $2\times2°\times50$ km. The ak135 model [17] was used as the reference. In order to account for the large residuals associated with paths through ancient shields and mantle plumes we include well-associated phases with residuals from ak135 up to ±7 s for P waves and ±25 s for S waves. The resulting dataset for the joint inversion contains 900 000 pairs of P and S ray paths.

The broad span of residuals is designed to capture the spread of residuals associated with the zones of major heterogeneity at the top and bottom of the mantle. In the epicentral distance range from 30° to 80° fewer than 70 observations, out of more than 650 000, have S residuals greater

than 11 s and in consequence there is negligible impact on the images from maintaining the broad bounds.

The technique of joint bulk-sound and shear wave-speed tomography for arrival-time data was introduced by [10] and our inversion algorithm is based on this formulation. The main improvement is the application of 3-D ray tracing [18] to take into account the influence of 3-D Earth structure on the trajectory of seismic-ray propagation in passage from source to receiver. This ray-tracing scheme has been tested and successfully applied for global tomography for P waves [9] and for S waves [19]. The tomographic inversion was undertaken with a nested iterative approach. The first stage was to estimate 3-D models for P and S wave speed using conventional linearized travel-time inversion. The resulting P and S models were taken as starting models for the subsequent non-linear joint tomographic inversion for bulk-sound and shear wave speed. Three-dimensional ray tracing was carried out

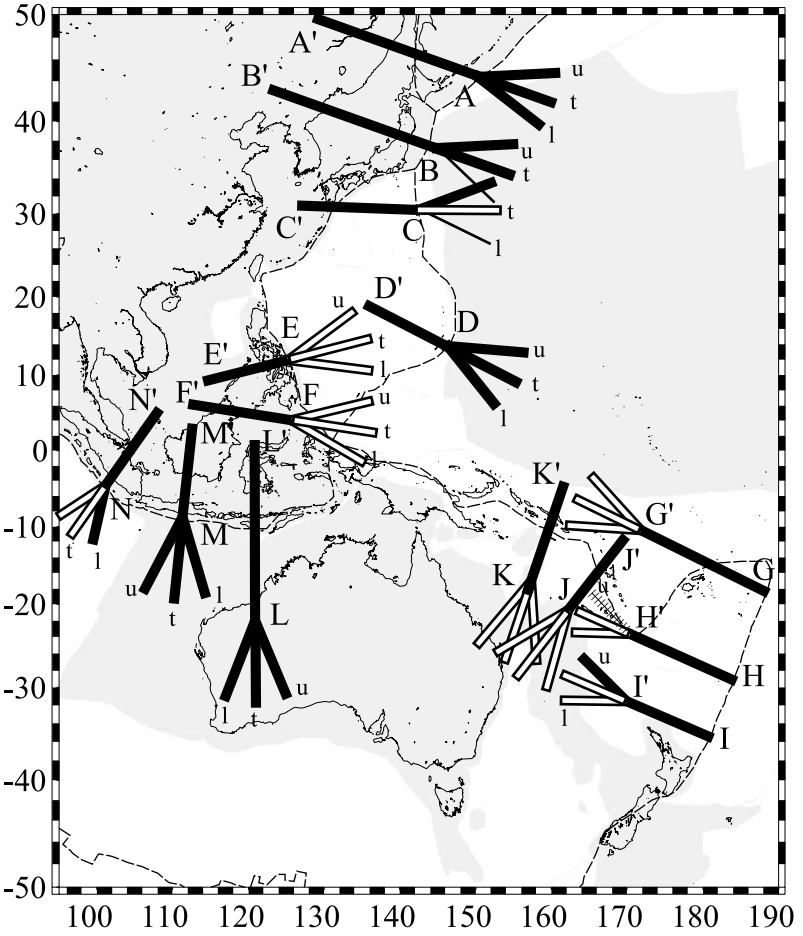

Fig. 1. Location of the cross-sections of the dual tomographic images discussed in the text. Summary of the relative behavior of the bulk-sound speed and shear wave speed through the Western Pacific subduction zones is presented by bars. Three bars are shown for each section, representing the upper mantle, transition zone and lower mantle (denoted u, t, l for clarity). The bars are white if bulk-sound is dominant, black if shear wave speed dominates, and a broken bar indicates similar amplitude anomalies. A thin line for the lower mantle indicates no evident penetration. Shaded gray zones on the seafloor indicate areas older than 100 Ma, according to [27].

through P and S models derived in the first stage. The joint inversion uses the P and S arrival-time datasets simultaneously using the approach detailed in the appendix to [10]. The iterative scheme works alternately with sets of linear equations focused on bulk-sound speed or shear wave speed, with linkage between the equation sets introduced by successive updates of cross-coupling terms. The decrease in variance reduction was approximately 1% between the third and fourth iteration of this linked inversion scheme with no visual change in the resulting image, and so the process was terminated at the fourth iteration. The solution of the large individual sets of linear equations with sparse matrices was carried out using the LINBCG method (iterative biconjugate gradient solution). The initial and joint inversions for regional and global structures were performed simultaneously to minimize the influence of the surrounding structures on the image of the Western Pacific region.

Even with the joint inversion for bulk-sound speed and shear wave speed we have to take care to ensure that the tomographic images can be directly compared. We have selected P and S data with common source–receiver pairs so the ray paths will be similar, and because of the difference in frequency between P and S arrivals the wavelengths employed will be close. However, there is some potential for frequency-dependent influences in regions of low Q. We therefore focus attention on the high wave-speed anomalies corresponding to the subducted slabs, which are expected to be colder than their environment in the mantle and have high Q.

3. Bulk-sound and shear wave-speed anomalies

Numerous tomographic inversions have been performed focusing on the structure of the Western Pacific subduction zones (e.g. [2,20–22]). Our tomographic results, in general, are in good agreement with those studies. Therefore, our main attention will be focused on the balance between bulk-sound and shear wave-speed amplitudes and we will pay less attention to the shape of the high-velocity anomalies associated with the subducted slab of well-known subduction zones that have been widely described in previous studies. We will use a consistent nomenclature for the parts of the mantle: the *uppermost mantle* extends from the Earth's crust down to a depth of 410 km, the *transition zone* covers the depth range from 410 to 660 km, and the *lower mantle* lies below a depth of 660 km.

We illustrate the variations in the character of the subduction processes in the Western Pacific with cross-sections across the different subduction zones. We start with subduction in the northwest Pacific and then consider subduction in the southwest Pacific and Indonesian regions (Fig. 1).

3.1. Kurile

The Kurile convergent boundary is characterized by subduction of the Pacific plate of Late Cretaceous age (e.g. [23,24]). Deep penetration of the subducting slab into the Earth's mantle down to a depth of ~1000 km was previously reported by [9] and [25]. This deep slab penetration can also be seen in our tomographic models (Fig. 2). The amplitude of the slab signal in shear wave speed is more pronounced in the upper mantle than for bulk-sound speed. Although the upper surface of the slab is similar in the two images, we see some differences in the morphology of the slab. This suggests that we are seeing some difference in the character of the physical properties within the slab in the upper mantle. The slab can be tracked in both images into the lower mantle.

3.2. Japan

The subduction of the Pacific plate below the Japanese islands has been studied in numerous tomographic researches (e.g. [20,22]). The average age of the descending plate is Early Cretaceous (e.g. [23,24]) and the slab can be mapped down to a depth of ~660 km with some flattening in the mantle transition zone. The amplitude of the fast shear wave-speed anomaly associated with the Pacific plate is noticeably higher than that for bulk-sound along the whole length of the subducted slab.

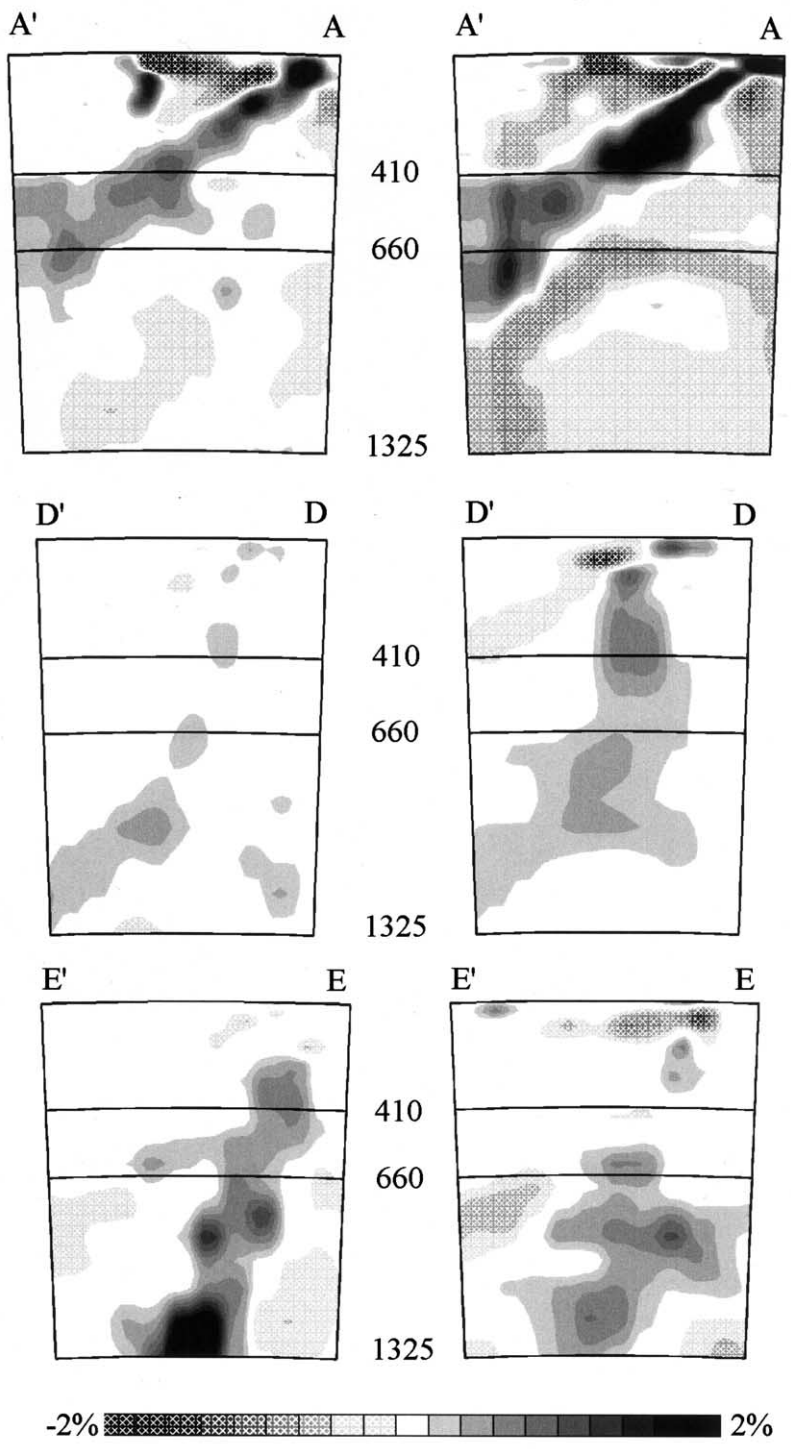

Fig. 2. Cross-sections through the bulk-sound speed (left column) and shear wave-speed (right column) models for the northwestern Pacific region: (AA′) Kurile arc, (DD′) Mariana arc, (EE′) Philippine arc.

3.3. Izu–Bonin

The Izu–Bonin region presents a striking example of a stagnant slab with a substantial horizontal portion lying on top of the 660 km discontinuity. Widiyantoro et al. [13] have used separate P and S tomographic images to argue for a change in the physical properties of the subducting material in the stagnant slab. The flat portion of the subducted Pacific slab shows a much more distinct fast anomaly in P wave speed than for S wave speed. This was interpreted in terms of a stronger contribution from the bulk-sound speed because of low flexural rigidity, while the part of the slab penetrating the 660 km discontinuity is more rigid and pronounced in the shear wave speed.

The influence of 3-D ray tracing and the iterative non-linear inversion on the joint tomography can be judged by comparison with images computed using a single-pass linearized inversion with ray tracing through just the 1-D reference model (Fig. 3). The results from many different facets of the models indicate that the single-pass inversion generally underestimates velocity perturbations by about 30% compared with a 3-D inversion with the same inversion parameters. The 3-D ray-tracing tomography also produces sharper images than those obtained with 1-D ray tracing. These differences at the regional scale are similar to the results presented by [9] and [19] for global tomography. The relative behavior between the bulk-sound and shear wave-speed anomalies is similar in both inversions. Our tomographic images (Fig. 3) along the same section through the Izu–Bonin and Ryukyu arcs support these results. In each case they show a more pronounced feature in bulk-sound speed for the subducted structures accumulated above the 660 km discontinuity. The fast anomaly for the shear wave speed in the Pacific slab in the Izu–Bonin arc is rather strong in the upper mantle and into the transition zone before the point of flexure. The Ryukyu arc has a very distinct fast shear wave-speed anomaly down to about 300 km and then stops rather abruptly, with a possible slight extension in the bulk-sound speed image. However, we find larger differences between the two wave speeds in the lower mantle

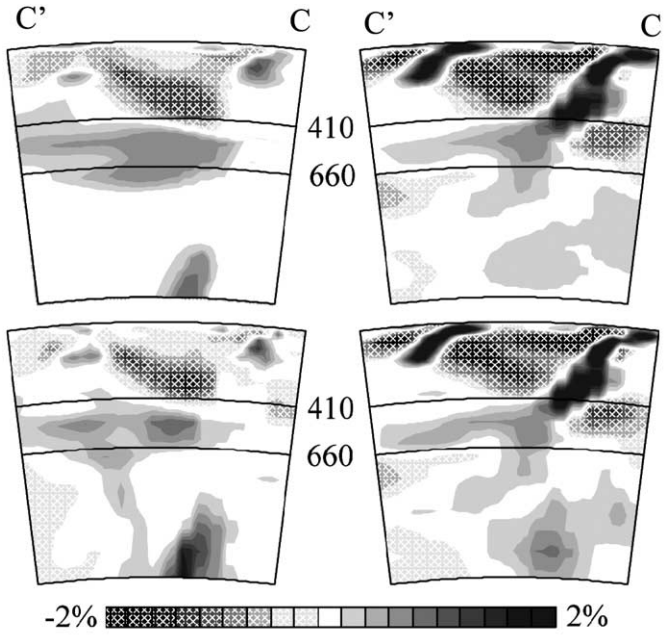

Fig. 3. Cross-section through the bulk-sound (left column) and shear wave-speed (right column) models for the Izu–Bonin and Ryukyu arcs following the line of section of [13]. The upper row of sections represents the inversion with the standard one-dimensional ray-tracing approach, while the lower row uses the three-dimensional ray tracing in an iterative non-linear inversion.

images that we use to judge the possible penetration of the Pacific plate. The amplitudes of the heterogeneity are similar with slightly faster values than for the ak135 reference model. However, the shear wave-speed anomalies seem to form a linear extension of the subducted slab along the dip plane, while the bulk-sound anomalies extend down to the mid-mantle starting approximately from the center of the area formed by accumulated material above the 660 km discontinuity. A low-amplitude fast zone in shear wave speed spreading across the image at a depth of ~1000 km is not visible on the bulk-sound image.

3.4. Mariana

The zone of elevated wave speeds below the Mariana trench (Fig. 2) extends down through the lower mantle at least to a depth of ~1500 km, which represents the base of our detailed regional mesh. Synthetic resolution tests suggest that our inversion should be able to recover such a feature in both bulk-sound and shear wave speed to the base of this grid.

The amplitudes of the fast bulk-sound and shear wave-speed anomalies are somewhat muted compared with the Izu–Bonin zone to the north, but are detectable along the full depth of the slab. The subducted slab is of Jurassic age [26] and shear wave-speed anomalies are dominant throughout. Similar results were reported by [13] based on separate inversions for P and S tomographic images. Low-amplitude high-velocity anomalies, spreading at a depth of ~1000 km around the subducted slab can be seen on the shear wave tomographic image. This feature is not as evident in the bulk-sound image.

3.5. Philippines

The southwest Philippine plate of Eocene age [27] descends westward beneath the Philippines trench at a rate of ~80 mm/yr. The location of the trench has not changed significantly during the last 25 Myr, with almost half of the Philippine plate consumed by subduction [28]. Traces of the subducted slab are visible down to a depth of ~1500 km (the bottom of the regional parame-

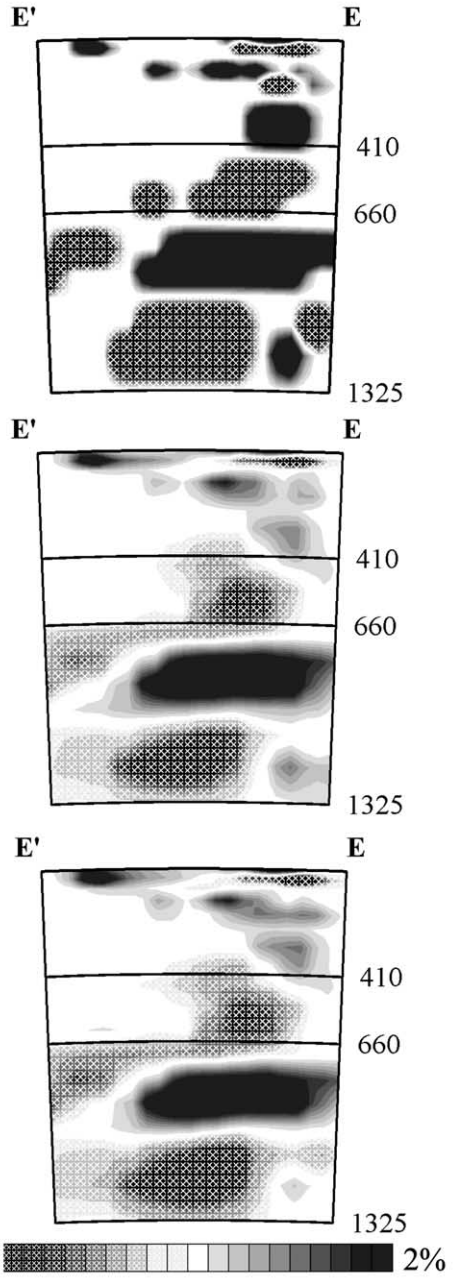

Fig. 4. Resolution calculations for the Philippine arc structure. The initial synthetic model is presented in the uppermost cross-section. Middle and lower cross-sections show the recovery of the synthetic model for bulk-sound and shear wave speed, from P and S times contaminated with random noise.

terization model) on both the bulk-sound and shear wave-speed tomographic images (Fig. 2). Resolution tests (Fig. 4) suggest that the image of subducted slab can be recovered along its complete extension. Moreover, the velocity anomaly structures visible on the bulk-sound images can be retrieved in the shear wave speed with the same amplitude and vice versa.

The following approach was adopted to test the seismic-velocity anomalies. A synthetic Earth model was constructed for the resolution tests with a wavelength of seismic-velocity anomalies matching that of the joint inversion for both bulk-sound and shear wave speeds. This common single synthetic model contains the features visible in both bulk-sound and shear models. Therefore we can test the two classes of structures simultaneously. For each cell where the inversions indicate high-velocity perturbations are greater than 0.5%, a 2% deviation was assigned automatically to each wave speed. The sign of the perturbations was changed for each pair of layers, separated by a blank layer, to create a pseudo-checkerboard pattern (Fig. 4). The ray paths corresponding to the source–receiver pairs used for the observations were retraced through the synthetic model. The corresponding travel times were used in the joint tomographic inversion with the addition of normally distributed noise with a variance of 1 s^2 for P waves and 2.25 s^2 for S waves. The recovered models from this noisy data are displayed in Fig. 4 for both bulk-sound speed and shear wave speed. The same inversion parameters were used for this resolution test as were used in the joint tomographic inversion using the observed data. This approach allows us to detect differences in the models arising from the differences in the ray path coverage between P and S data. The resolution tests show that the recovered synthetic models are nearly identical, indicating that differences between bulk-sound and shear models are dominated by the information contained in the travel times and the differences in the ray paths for P and S data are not significant.

The Philippine slab is difficult to pick up close to the surface but from 200 km downwards shows a clear set of fast wave-speed features. In this region the bulk-sound component is more distinct than the shear wave-speed anomalies, particularly in the upper mantle and the transition zone. We note that the configuration of the fast wave speeds for the two wave types is somewhat different in the lower mantle. A broadening of the shear wave-speed anomalies is seen above a depth of $\sim$1000 km, but does not have a counterpart in the bulk-sound image.

3.6. Tonga–Kermadec

Although magnetic anomalies near the Tonga–Kermadec subduction zone have not been determined north of 16°S, the age of the Pacific plate can be assumed to be approximately 170 Ma [29]. Fast rollback of the trench (by about 160 mm/yr, [30]) may have significantly altered the normal mechanics of the subduction process, which is characterized by a convergence rate of approximately 80 mm/yr between Australian and Pacific plates [31]. Widiyantoro et al. [13] suggest that the retreat of the trench can affect the physical properties of the subducted slab and, therefore, the balance between amplitudes of bulk-sound speed and shear wave-speed anomalies. Since the rate of the trench rollback is maximum at the northern end of Tonga and minimum at the southern extremity (Kermadec), the balance between the two wave speeds would therefore be expected to vary significantly from north to south along the trench.

Our joint tomographic images for the northern Tonga to Fiji region (Fig. 5) show a prominent bulk-sound high-velocity anomaly extending down to the 660 km discontinuity with flattening in the transition zone. This bending and flattening of the slab in the transition zone can be induced by trench rollback, as suggested by numerous authors (e.g. [32–34]). A further bulk-sound high-velocity zone extension is traced down to the bottom limits of the tomographic model (Fig. 5) and is a resolved feature (Fig. 6). Shear wave-speed anomalies associated with the subducted slab are weak in this northern zone and can be seen only in the uppermost mantle and do not reach the boundaries of the transition zone.

The cross-section through the central part of the Tonga subduction zone (Fig. 5) reveals the

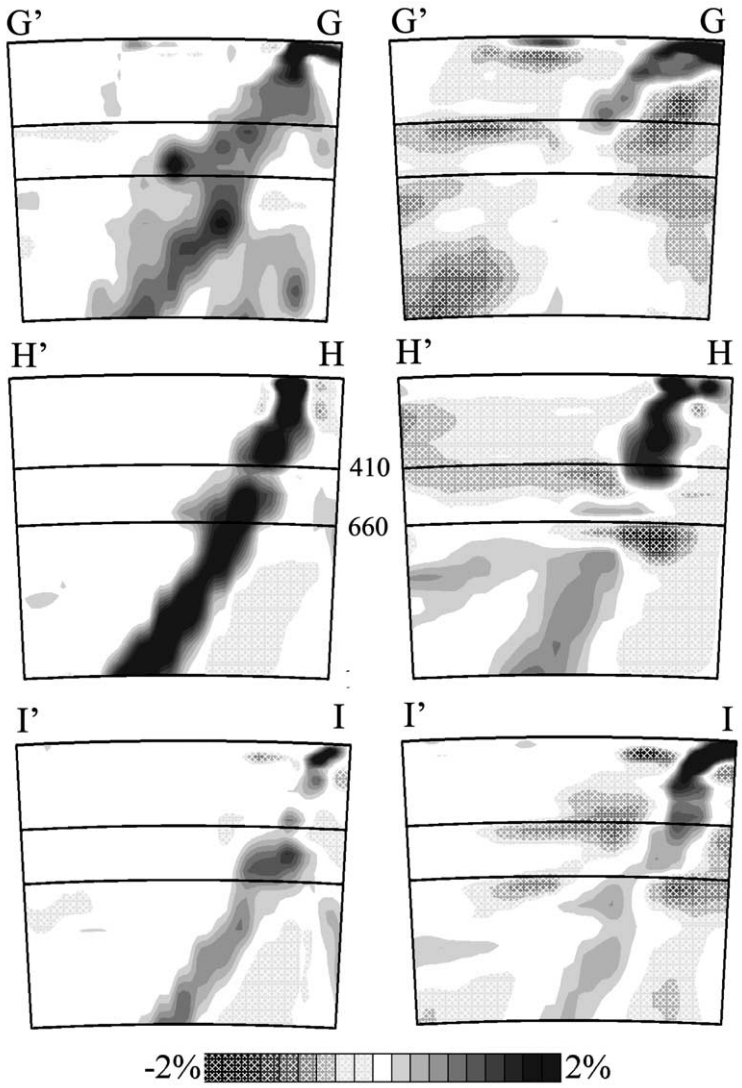

Fig. 5. Cross-sections through the bulk-sound speed (left column) and shear wave-speed (right column) models for the southwestern Pacific region: (GG′) Fiji region, (HH′) Tonga region, (II′) Kermadec region.

presence of a fast shear wave-speed anomaly along with the elevated bulk-sound speed. Although the bulk-sound anomaly is more prominent, the shape of the shear wave-speed anomaly corresponds to that of bulk-sound along the full extent of the slab. Some spreading of the shear high-velocity zone is detected above a depth of ~1000 km. The resolution calculations in Fig. 6 indicate that once again there should be good resolution of the nature of the slab.

The southernmost cross-section (Fig. 5) across the Kermadec subduction zone is characterized by a stronger anomaly in shear wave speed in the upper mantle and a weakening of the bulk-sound speed feature compared with the previous two cross-sections in Fig. 5. Resolution tests show good recovery for seismic-velocity anomalies associated with the subducted slab (Fig. 6). Both bulk-sound and shear wave-speed anomalies can be retrieved with the same amplitude. Although

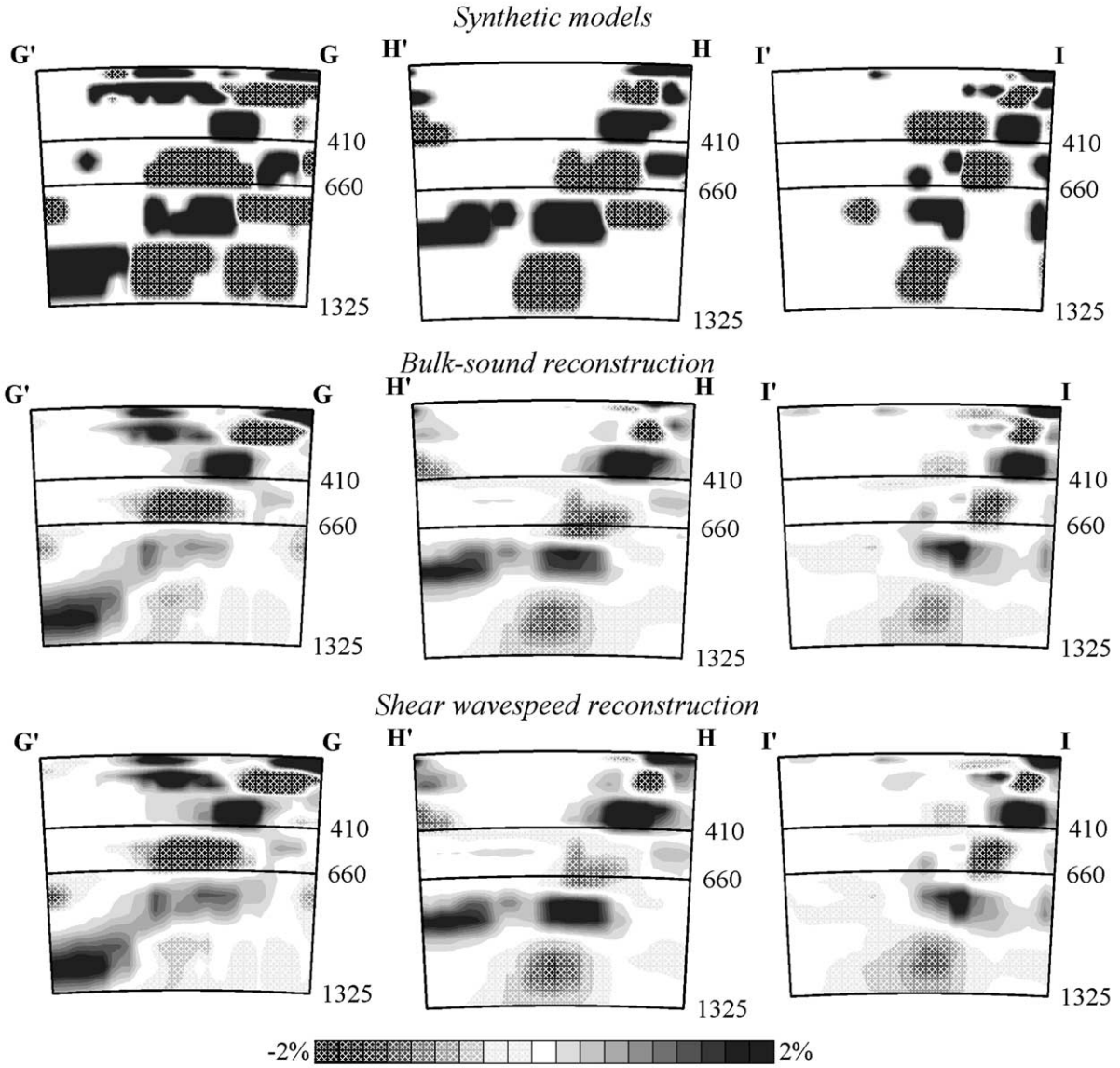

Fig. 6. Resolution tests for the Fiji–Tonga–Kermadec subduction zone. The uppermost row represents the cross-sections through the initial synthetic model. The middle and lower rows are the cross-sections through the recovered bulk-sound and shear wave-speed structures.

some smearing is observed around the area of plate penetration in the bulk-sound and shear wave-speed images, this smearing has similar values and behavior in both images and, therefore, cannot bias our comparisons. One useful measure of the data coverage available for the inversion is given by the density of ray paths. A convenient measure of this quantity is the sum of the lengths of ray segments traversing each cell (Fig. 7). For the Fiji–Tonga region there is a very consistent and high ray density across the regions where subduction-related structures might be expected. Nevertheless, the resolution tests show that the amplitude of the velocity perturbations in the low-

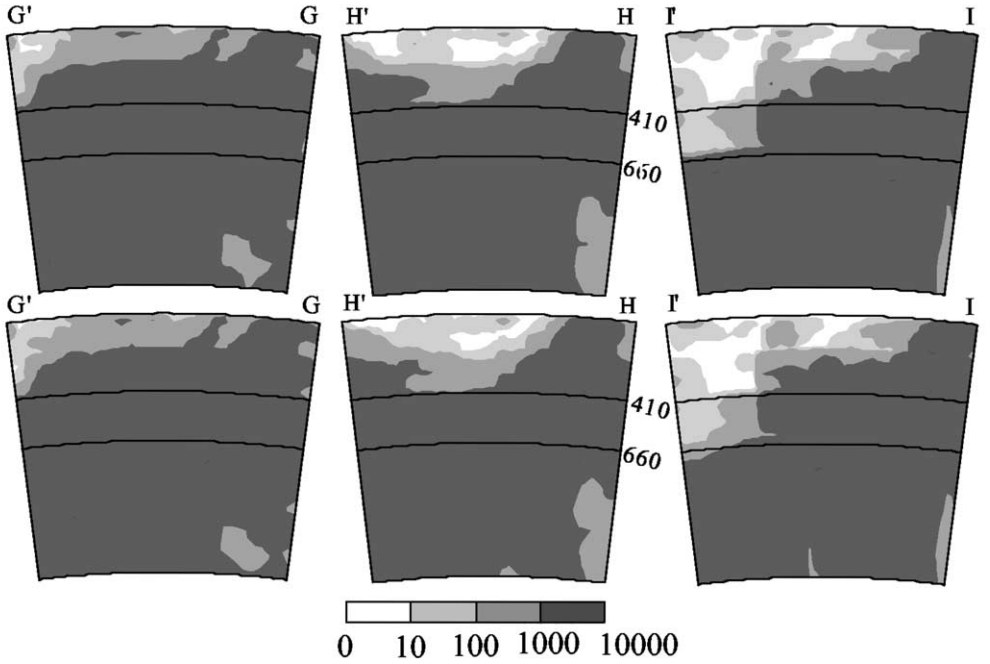

Fig. 7. Cross sections representing the density of ray-length segments (in km) for P wave (upper row) and S wave seismic rays (lower row) for the cross-sections shown in Fig. 5.

er mantle is likely to be somewhat underestimated.

3.7. New Hebrides

The New Hebrides subduction zone was initiated at about 10 Ma with opening of the North Fiji basin and cessation of southwest subduction along the Melanesian arc [35]. Paleomagnetic studies suggest an age of ~50 Ma [36] for the lithosphere subducted at the trench in this zone.

A high-velocity zone, which can be associated with the subducted slab, is observed down to a depth of about 1000 km (Fig. 8). The bulk-sound component is dominant for the full extent of the subducted slab. Weak traces of a fast shear wave anomaly are only seen in the transition zone and mid-mantle. The subducted slab in the uppermost mantle dips in the northeast direction, as expected from the present tectonic framework. The maximum depth of penetration also fits the present subduction velocity of ~80–90 mm/yr for 10 Myr of subduction history. However, the high-velocity anomalies in the transition zone and mid-mantle are oriented in the opposite, southwest direction. We speculate that this bending of the slab could reflect strong mantle flow associated with the opening of the North Fiji basin.

3.8. Solomon Islands

The northeast boundary of the Australian plate was formed about 40 Myr ago by numerous rifting processes [37]. The structure of the region is further complicated by the collision of the Ontong–Java plateau with the arc system [35]. The tomographic images from the joint inversion (Fig. 8) show a high-velocity zone dipping northeast down to a depth of about 1000 km. The fast features in the bulk-sound image are more prominent than those of the shear wave speed, which are weak and have a scattered distribution.

3.9. Molucca

The tectonics of the area around the Molucca

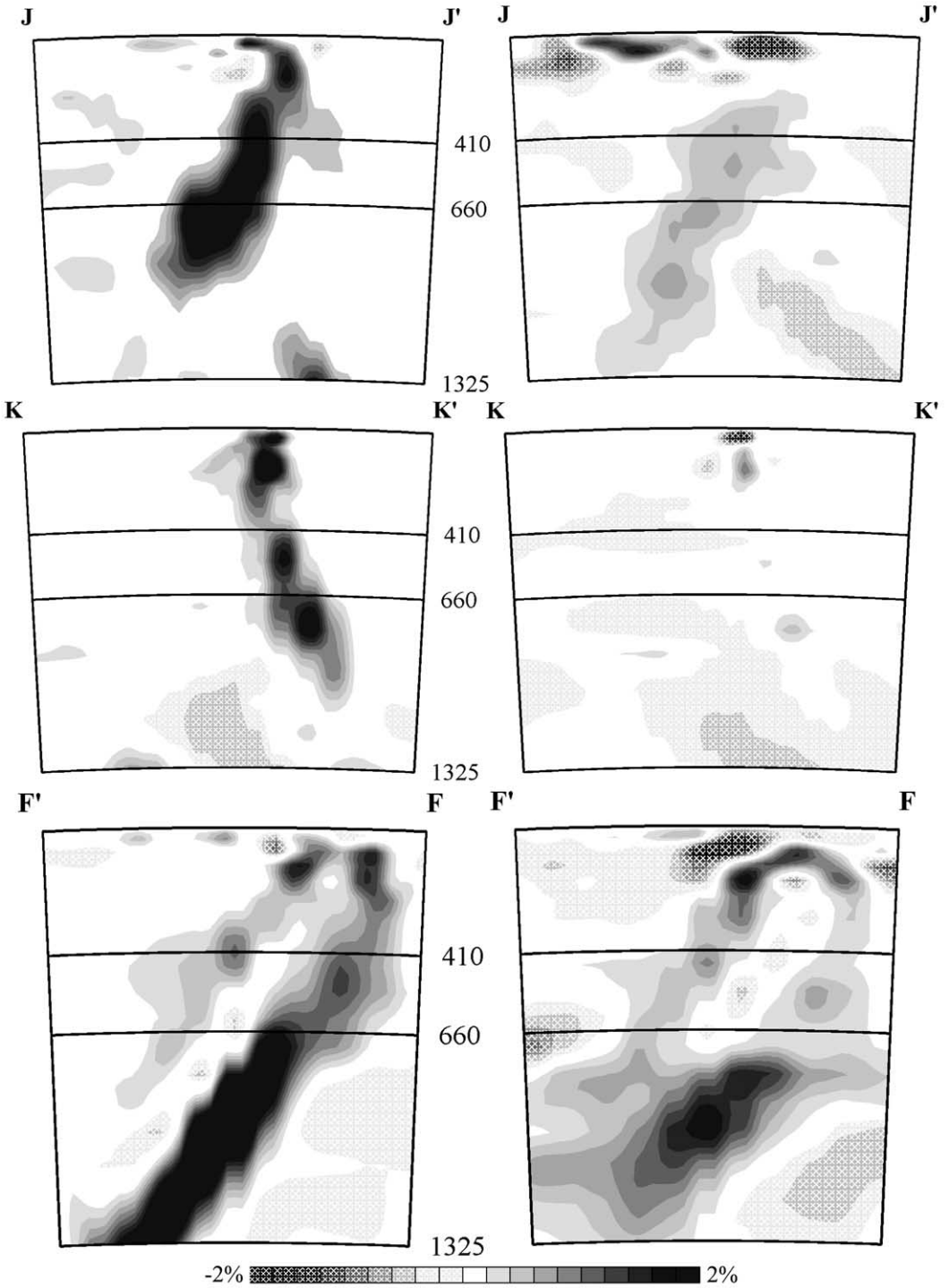

Fig. 8. Cross-sections through the bulk-sound speed and shear wave-speed models for the southwestern Pacific region: (JJ′) New Hebrides arc, (KK′) Solomon arc, (FF′) Molucca region.

Sea involves numerous small plates and plate boundaries that have shifted and evolved on timescales of a few million years [28,35]. Our tomographic images (Fig. 8) show two sub-parallel zones of fast wave speed descending deep into the mid-mantle down to depths of about 1500 km for the right-hand sheet and about 900 km for the left-hand sheet, which form an inverted U-shape anomaly. This double-sheet zone of elevated seismic velocities can be associated with the Molucca Sea plate [38] bordered by Sangihe and Halmahera arcs. The Molucca Sea plate has largely been subducted and has been overridden by the Halmahera arc [35]. The configuration of the 3-D seismic wave-speed structures in this region is rather complex and simple 2-D cross-sections can be quite misleading. The shallow seismicity down to depths of 200–300 km below the Halmahera arc [38] is associated with the easterly dipping segment of the slab, which is clearly visible in the shear wave-speed image. The deepest seismicity to about 600 km depth corresponds to the slab subducted below the Sangihe arc (left-hand sheet) [38].

There is a strong, fast anomaly in bulk-sound speed below the Halmahera arc with a westerly dip, although the clear, shallow shear wave anomaly shows an easterly dip correlating with the seismicity. The westerly dipping component at depth is comparatively weak, particularly in the transition zone. In contrast, a very similar behavior for the two wave types is seen below the Sangihe arc. Spreading of the fast shear wave-speed anomaly can be seen around a depth of 800 km.

3.10. Java–Sumatra

The Java–Timor subduction zone is characterized by collision between Australian and Asian plates and subduction of terrains associated with the Australian plate. At Timor itself present-day subduction has initiated beneath the Australian plate as buoyant continental material associated with the ancient Australian craton appears to have blocked the former subduction [35].

In the Java region, fast zones of shear wave speed associated with the subducted slab are most prominent in the uppermost mantle and within the transition zone. However, below the transition zone down to the maximum depth of the regional tomographic model the bulk-sound signature is dominant. The zone of fast shear wave speed extends down to a depth of about 1500 km with northward flattening above a depth of $\sim$1000 km. The combination of the bulk-sound and shear wave-speed anomalies creates a

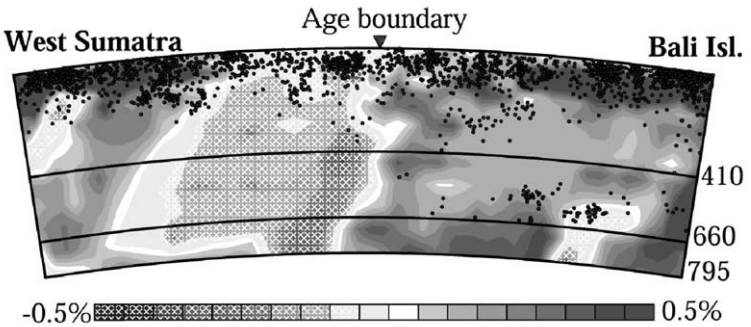

Fig. 9. The variation in the relative average amplitude of the bulk-sound speed and shear wave-speed anomalies along the subducted plate in the Java–Sumatra subduction zone. The cells with high-velocity anomalies associated with the subducted plate were isolated and averages made through the thickness of the plate of the difference between the wave-speed variations from the ak135 reference model [17]. The bulk-sound speed values are subtracted from the shear wave-speed values, and the results are then projected on the vertical section. Thus large bulk-sound velocity anomalies appear as negative values (patterned gray tone), while high shear wave speed is presented as positive anomaly (solid gray tone). The points where the age of the seafloor changes are indicated and show a strong correlation with the changes in the balance between the two wave types. Solid black dots are seismic hypocenters.

tomographic image for P wave speed of the subducted plate that is similar to the results of [39]. A strong shear signature of the slab below the Java subduction zone was noted in [13].

Further west, where the Australian plate of Late Cretaceous age [40] subducts below Sumatra, the amplitude of the shear wave-speed anomaly abruptly decreases. Flattened segments of the shear wave anomaly are not observed in the mid-mantle. In this area the slab is marked out by elevated bulk-sound speeds from the uppermost mantle down to the middle of the transition zone.

The variation along the arc is most clearly seen by projecting the relative amplitude of the bulk-sound and shear wave-speed anomalies onto the depth variation of the slab (Fig. 9). The difference between the variations in the bulk-sound speed and shear wave speed from the ak135 reference model [17] is constructed on a cell-by-cell basis for the high-velocity anomalies associated with subduction and then projected onto the subduction zone. The very distinct changes in the relative behavior of the two wave types correspond closely to where there is a change in the age of the subducted seafloor determined from significant shifts in the patterns of magnetic anomalies [35].

4. Discussion and conclusions

The results from our joint bulk-sound and shear wave-speed tomographic inversion strongly support earlier observations [13] that variations in the amplitude ratio between the two wave types, and hence a difference in physical properties, occur in the portions of the subducted slabs that are deflected above the 660 km discontinuity or which penetrate into the lower mantle. Subducted slabs deflected above the 660 km discontinuity, such as in the Izu–Bonin or Tonga subduction zones, are usually associated with strong, fast bulk-sound anomalies accompanied by only slightly fast shear wave-speed variations. Several scenarios for bulk-sound dominance in the deflected slabs were discussed by [13], who concluded that the strong bulk-sound perturbations but little signature in S imply low rigidity, while the slab fragments that show clear penetration into the lower mantle have a strong shear signature.

However, our tomographic models clearly show that the slabs that penetrate deep into the low mantle (Philippine, Solomon, New Hebrides) can still be dominated by the bulk-sound perturbation, whereas a significant shear wave-speed signature exists in the deflected slab below Japan. These new results suggest that the deflection or penetration of the slab is not the only indicator of the prominence of the bulk-sound or shear wave speeds within the subducted slabs.

We need to seek a reason for a change of physical properties in the slab and so we analyze the spreading history for the subducted slabs at the trench and try to relate it to the dominance of the bulk-sound or shear wave-speed anomalies. Only wave-speed anomalies in the uppermost mantle are used to simplify interpretation and to reduce the influence of the older (and hidden) spreading history of the slab.

Generally, subducted slabs that have not been affected by strong present-day trench migration are more pronounced in shear wave speed if the subducted crust at the trench is older than about 90 Ma. Pronounced bulk-sound anomalies are more common for younger slabs or those affected by fast trench retreat regardless of their flattening above or penetration through the 660 km discontinuity.

When we consider those subduction zones which are not affected by trench rollback we find that they separate into two groups. The first group, dominated by shear wave speed, mostly consists of the old Pacific slabs below Kuriles, Japan, Mariana, and Kermadec. The second group, dominated by bulk-sound, includes Philippine, New Hebrides, Solomon and Sumatra subduction zones. The noticeable changes with the age of the subducted material along the Sumatra–Java arc are consistent with these results. It would appear that oceanic lithosphere older than 90 Ma, which has reached full thickness and thermal maturity, has also begun to modify its physical properties. It is possible that this arises through the influence of anisotropy, which would map into wave-speed variations in the joint inversion based on an isotropic model.

The Izu–Bonin and Tonga subduction zones are clearly affected by fast trench retreat and show dominance of bulk-sound variations as reported by [13]. Although the strong influence of the trench rollback on the physical properties of the subducted slab (reflected in the dominance of the bulk-sound) is confirmed by our study, the detailed analysis of the Tonga–Kermadec subduction zone reveals additional details of this phenomenon.

The images of the fast wave speeds associated with the subducted Pacific plate below northern Tonga are dominated by a bulk-sound anomaly along the full extent of the slab from the uppermost mantle to the lower mantle, both for the flattened as well as the penetrating portions of the subducted slabs. The shear wave anomaly is only visible in the uppermost mantle. This observation suggests that the apparently reduced rigidity of the slab does not prevent slab penetration into the lower mantle. The part of the slab flattening above the 660 km discontinuity could correspond to the split metastable wedge of the former oceanic lithosphere [13]. In the southern portion of the same subduction system near Kermadec, which is much less affected by trench rollback, we find the fast wave speeds dominated by shear structure in the upper mantle. From our results for the other subduction zones, this is what would be expected for the age of ~170 Ma of the Pacific plate at the trench. Thus, the mechanical influence of fast trench retreat can significantly affect the physical parameters of the slab and, therefore, be detected by joint bulk-sound and shear wave-speed tomography.

The relative behavior of the bulk-sound speed and shear wave speed through the Western Pacific subduction zones is summarized in Fig. 1, in terms of the behavior of a number of different cross-sections. All these observations suggest that the physical properties of the subducting plate relate to the age of the subducted slab. The information on the properties of the uppermost mantle from the sections in Fig. 1 is replotted as a function of the age of the seafloor at the trench in Fig. 10. With the exception of the north Philippine region, where there is considerable uncertainty in the age of the seafloor, there is a clear

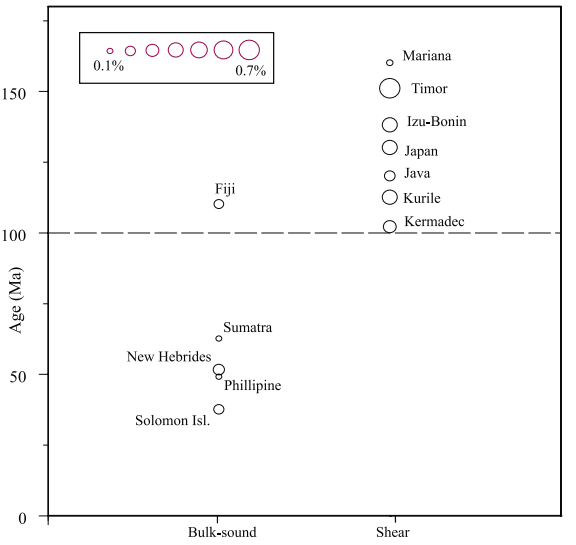

Fig. 10. Summary of the relative behavior of the bulk-sound and shear wave speed in the upper mantle as a function of the age of the seafloor at the trench. The size of the ball represents the average value of the dominance of one modulus compared with the other within the subducted plate (the scale is shown in the inset). Velocity perturbations within a band 300 km wide around the individual cross-sections were selected for the analysis.

separation between bulk-sound speed dominance for younger slabs (<90 Ma) and shear wave-speed dominance for older slabs (>90 Ma).

A similar dependence on the age of the subducted lithosphere was proposed for the relationship between the maximum depth of seismicity and the thermal parameters of the subducted plate (e.g. [41]). The similarities between the two phenomena can be illustrated by the Java–Sumatra subduction zone, where the amplitude ratio between the bulk-sound and shear wave speed correlates with the maximum depth of seismicity (cf. Fig. 9).

Another prominent feature revealed in our study is a flattened zone of elevated shear wave speed between 800 and 1000 km around the regions where subducted slabs penetrate deeply into the lower mantle. There is no comparable feature in the bulk-sound speed images. Frequently, a depth close to 1000 km is regarded as the bottom of the transition zone near subduction zones [42]. Seismic anomalies near 1000 km depth have been reported by [43] from ScS reverberations and by

[44–46] from direct observations of the converted phases below the Western Pacific region. Although these seismic anomalies are not accepted as a general attribute of the lower mantle, these direct observations could be related to the zone of elevated shear wave speed detected in our tomographic inversion. There is a possible explanation of discontinuities near 900 km depth in terms of changes in the symmetry of silicate perovskite crystals [43]. The detection of this ~900 km discontinuity only within the Western Pacific region might be explained by the presence of deep subduction in this region; slab penetration into the lower mantle could introduce chemical or thermal disequilibria relative to the surrounding mantle at a depth of ~900 km, with strongest effects on the shear wave speed.

Acknowledgements

We thank three anonymous reviewers for valuable suggestions which greatly improved the manuscript. We are indebted to A. Limaye for help in creating the visualization software used for this study and the Australian Partnership for Advanced Computing (APAC) for providing excellent computer facilities.*[SK]*

References

[1] K. Aki, W.H.K. Lee, Determination of three-dimensional velocity anomalies under a seismic array using first P arrival times from local earthquakes, J. Geophys. Res. 81 (1976) 4381–4399.
[2] H. Bijwaard, W. Spakman, E.R. Engdahl, Closing the gap between regional and global travel time tomography, J. Geophys. Res. 103 (1998) 30055–30078.
[3] A. Gorbatov, Y. Fukao, S. Widiyantoro, Application of a three-dimensional ray-tracing technique to global P, PP and Pdiff traveltime tomography, Geophys. J. Int. 146 (2001) 583–593.
[4] H. Karason, R.D. van der Hilst, Mantle P-wave speed from seismic tomography: advances in methodology and data integration, IAGA-IASPEI symposia abstracts, Vietnam, 2001, p. 358.
[5] A.M. Dziewonski, Mapping the lower mantle: Determination of lateral heterogeneity in P velocity up to degree and order 6, J. Geophys. Res. 89 (1984) 5929–5952.
[6] S.P. Grand, R.D. van der Hilst, S. Widiyantoro, Global seismic tomography: A snapshot of convection in the Earth, GSA Today 7 (1997) 1–7.
[7] S. Widiyantoro, B.L.N. Kennett, R.D. van der Hilst, Extending shear-wave tomography for the lower mantle using S and SKS arrival-time data, Earth Planet. Space 50 (1998) 999–1012.
[8] D.W. Vasco, L.R. Johnson, Whole earth structure estimated from seismic arrival times, J. Geophys. Res. 103 (1998) 2633–2671.
[9] A. Gorbatov, S. Widiyantoro, Y. Fukao, E. Gordeev, Signature of remnant slabs in the North Pacific from P-wave tomography, Geophys. J. Int. 142 (2000) 27–36.
[10] B.L.N. Kennett, S. Widiyantoro, R.D. van der Hilst, Joint seismic tomography for bulk-sound and shear wavespeed in the Earth's mantle, J. Geophys. Res. 103 (1998) 12469–12493.
[11] R.D. van der Hilst, H. Karason, Compositional heterogeneity in bottom 1000 kilometers of Earth's mantle: toward a hybrid convection model, Science 283 (1999) 1885–1888.
[12] H.-C. Nataf, Seismic imaging of mantle plumes, Annu. Rev. Earth Planet. Sci. 28 (2000) 391–417.
[13] S. Widiyantoro, B.L.N. Kennett, R.D. van der Hilst, Seismic tomography with P and S data reveals lateral variations in the rigidity of deep slabs, Earth Planet. Sci. Lett. 173 (1999) 91–100.
[14] D. Zhao, H. Kanamori, N. Hiroaki, D. Wiens, Tomography of the source area of the 1995 Kobe earthquake: evidence for fluids at the hypocenter?, Science 274 (1996) 1891–1894.
[15] S. Kamiya, Y. Kobayashi, Seismological evidence for the existence of serpentinized wedge mantle, Geophys. Res. Lett. 27 (2000) 819–822.
[16] E.R. Engdahl, R.D. van der Hilst, R.P. Buland, Global teleseismic earthquake relocation with improved travel times and procedures for depth determination, Bull. Seism. Soc. Am. 88 (1998) 722–743.
[17] B.L.N. Kennett, E.R. Engdahl, R. Buland, Constraints on seismic velocities in the Earth from travel times, Geophys. J. Int. 122 (1995) 108–124.
[18] K. Koketsu, S. Sekine, Pseudo-bending method for three-dimensional seismic ray tracing in a spherical earth with discontinuities, Geophys. J. Int. 132 (1998) 339–346.
[19] S. Widiyantoro, A. Gorbatov, B.L.N. Kennett, Y. Fukao, Improving global shear wave traveltime tomography using three-dimensional ray tracing and iterative inversion, Geophys. J. Int. 141 (2000) 747–758.
[20] H. Inoue, Y. Fukao, K. Tanabe, Y. Ogata, Whole mantle P-wave travel-time tomography, Phys. Earth Planet. Inter. 59 (1990) 294–328.
[21] Y. Fukao, M. Obayashi, H. Inoue, M. Nenbai, Subducting slabs stagnant in the mantle transition zone, J. Geophys. Res. 97 (1992) 4809–4822.
[22] R.D. van der Hilst, S. Widiyantoro, E.R. Engdahl, Evidence for deep mantle circulation from global tomography, Nature 386 (1997) 578–584.

[23] M.L. Renkin, J.G. Sclater, Depth and age in the North Pacific, J. Geophys. Res. 93 (1988) 2919–2935.
[24] M. Nakanishi, K. Tamaki, K. Kobayashi, Mesozoic magnetic anomaly lineations and seafloor spreading history off the Northwestern Pacific, J. Geophys. Res. 94 (1989) 15437–15462.
[25] R.D. van der Hilst, E.R. Engdahl, W. Spakman, G. Nolet, Tomographic imaging of subducted lithosphere below northwest Pacific island arcs, Nature 353 (1991) 37–43.
[26] M. Nakanishi, K. Tamaki, K. Kobayashi, Magnetic anomaly lineations from Late Jurassic to Early Cretaceous in the west-central Pacific ocean, Geophys. J. Int. 109 (1992) 701–719.
[27] R.D. Mueller, W.R. Roest, J.-Y. Royer, L.M. Gahagan, J.G. Sclater, A digital age map of the ocean floor, SIO Reference Series 93-30, Scripps Inst. of Oceanography, Univ. of California at San Diego, La Jolla, CA, 1993.
[28] R. Hall, J.R. Ali, C.D. Anderson, Cenozoic motion of the Philippine Sea Plate: Paleomagnetic evidence from eastern Indonesia, Tectonics 14 (1995) 1117–1132.
[29] J.G. Sclater, C. Jaupart, D. Galson, The heat flow through oceanic and continental crust and the heat loss of the Earth, Rev. Geophys. Space Phys. 18 (1980) 269–311.
[30] M. Bevis et al., Geodetic observations of very rapid convergence and back-arc extension of the Tonga arc, Nature 374 (1995) 249–251.
[31] C. DeMets, Earthquake slip vectors and estimates of present-day plate motions, J. Geophys. Res. 98 (1993) 6703–6714.
[32] R.D. van der Hilst, T. Seno, Effects of relative plate motion on the deep structure and penetration depth of slabs below the Izu-Bonin and Mariana island arcs, Earth Planet. Sci. Lett. 120 (1993) 395–407.
[33] R.W. Griffiths, R.I. Hackney, R.D. van der Hilst, A laboratory investigation of effects of trench migration on the descent of subducted slabs, Earth Planet. Sci. Lett. 133 (1995) 1–17.
[34] U.R. Christensen, The influence of trench migration on slab penetration into the lower mantle, Earth Planet. Sci. Lett. 140 (1996) 27–39.
[35] R. Hall, Cenozoic geological and plate tectonic evolution of SE Asia and the SW Pacific: computer-based reconstructions, model and animations, J. Asian Earth Sci. 20 (2002) 353–431.
[36] B. M. Larue, J. Daniel, C. Jouannic, J. Recy, The south Rennel trough: evidence for a fossil spreading zone, in: Int. Symp. Geodynamics in South-West Pacific, Noumea, 1976, Editions Technip, Paris, 1977, pp. 51–62.
[37] K.A.W. Crook, L. Belbin, The Southwest Pacific area during the last 90 million years, J. Geol. Soc. Aust. 25 (1978) 23–40.
[38] R. McCaffrey, Lithospheric deformation within Molucca sea arc-arc collision: evidence from shallow and intermediate earthquake activity, J. Geophys. Res. 87 (1982) 3663–3678.
[39] S. Widiyantoro, R.D. van der Hilst, Mantle structure beneath Indonesia inferred from high-resolution tomographic imaging, Geophys. J. Int. 130 (1997) 167–182.
[40] Y.N. Neprochnov, L.R. Merklin, A.A. Shreyder, New data on the structure and geomagnetic field of the Sunda (Java) trench, Oceanology 19 (1979) 281–283.
[41] A. Gorbatov, V. Kostoglodov, Maximum depth of seismicity and thermal parameter of the subducting slab: general empirical relation and its application, Tectonophysics 277 (1997) 165–187.
[42] Y. Fukao, S. Widiyantoro, M. Obayashi, Stagnant slabs in the upper and lower mantle transition region, Rev. Geophys. 39 (2001) 291–323.
[43] J. Revenaugh, T.H. Jordan, Mantle layering from ScS reverberations 3: the upper mantle, J. Geophys. Res. 96 (1991) 19781–19810.
[44] H. Kawakatsu, F. Niu, Seismic evidence for a 920-km discontinuity in the mantle, Nature 6495 (1994) 301–305.
[45] F. Niu, H. Kawakatsu, Depth variation of the mid-mantle seismic discontinuity, Geophys. Res. Lett. 24 (1997) 429–432.
[46] L. Vinnik, F. Niu, H. Kawakatsu, Broadband converted phases from midmantle discontinuities, Earth Planet. Space 50 (1998) 987–997.